LNF-88/37

E. Burattini, G. Cappuccio, M.C. Ferrari, M. Grandolfo, P. Vecchia, Sh.M. Efendiev

MEDIUM INFRARED TRANSMITTANCE AND REFLECTANCE SPECTRA OF $Bi_{12}GeO_{20}$, $Bi_{12}SiO_{20}$, AND $Bi_{12}TiO_{20}$ SINGLE CRYSTALS

Estratto da: Op. Soc. of America B5, 714 (1988)

Reprinted from Journal of the Optical Society of America B, Vol. 5, page 714, March 1988

Medium infrared transmittance and reflectance spectra of $Bi_{12}GeO_{20}$, $Bi_{12}SiO_{20}$, and $Bi_{12}TiO_{20}$ single crystals

E. Burattini

Consiglio Nazionale delle Ricerche and Istituto di Fisica Nucleare, PWA Laboratory, c.p.13, 00044 Frascati, Italy

G. Cappuccio and M. C. Ferrari*

Consiglio Nazionale delle Ricerche, Istituto di Strutturistica Chimica, c.p.10, 00016 Monterotondo, Italy

M. Grandolfo and P. Vecchia

Istituto Superiore di Sanita'—Physics Laboratory, 00161 Rome, Italy

Sh. M. Efendiev

S. M. Kirov Azerbaijan State University, 370602 Baku, USSR

Received June 22, 1987; accepted September 24, 1987

Room-temperature infrared spectra of $Bi_{12}GeO_{20}$, $Bi_{12}SiO_{20}$, and $Bi_{12}TiO_{20}$ single crystals have been obtained in the energy range 2000–400 cm^{-1} (5–25 μm). In the transmission region from 2000 to 1000 cm^{-1} (5–10 μm), the band parameters have been determined through a best fit by Lorentz functions. For the analysis of the reflectance spectra in the range 1000–400 cm^{-1} (10–25 μm), instead of using the Kramers–Kronig relations, we preferred to use the classical oscillator method, which gives the best agreement with the experimental data. The determination of the oscillator parameters allowed us to deduce theoretical values for both the complex refractive index and the frequencies of TO and LO modes; the values for frequencies were in good agreement with those determined by other authors. The computational procedures are also presented and are critically discussed.

INTRODUCTION

Single crystals of $Bi_{12}GeO_{20}$ (BGO), $Bi_{12}SiO_{20}$ (BSO), and $Bi_{12}TiO_{20}$ (BTO) are attractive materials for various optical devices.[1–3] These materials belong to the group of sillenites with constant ratio, and their structure is described by the space group T^3 (I23). These compounds exhibit a number of remarkable properties: they are piezoelectric, electro-optical, elasto-optical, optically active, and photoconductive. The crystals can be large and can have excellent optical quality, which constitutes their main advantage over the other-known high-sensitivity electro-optical crystals. BTO differs slightly, however, in its optical and photoelectric properties[4,5] from those of similar compounds belonging to this group of crystals.

We have already presented the dispersion of the refractive index of BGO in the range 8400–2000 cm^{-1} at room temperature as the first step of a comprehensive study of the infrared optical properties of this kind of crystals.[6] In the present study we report infrared transmittance and reflectance measurements made on single-crystal BGO, BSO, and BTO samples. The measurements were made at room temperature in the spectral range 2000–400 cm^{-1}.

EXPERIMENTAL SETUP

BGO, BSO, and BTO crystals were grown following the Czochralski method. To achieve a good surface quality, after the cutting, the crystals' surfaces were finished by fine-carborundum grinding followed by fine-carborundum polishing. The composition and purity of all the samples were ascertained by electron-beam microprobe analysis.

Measurements were made by using two spectrophotometers: a Grubb-Parsons Spectromaster MK3 and a Perkin-Elmer 283-B. Both spectrophotometers are double-beam instruments with an optical null-balancing system based on comb attenuators. According to our previous measurements on BGO crystals,[6] a rotating sector disk attenuator was used to ensure a 99% accuracy in transmittance spectra.[7] A specifically designed accessory has been used for the specular reflectance measurements, and the precision achieved has been of the order of 95%, owing to the uncertainty in the indirect method used for the calibration of the reference gold mirror.[8]

The accuracy in wave-number values was 4 cm^{-1} for the Grubb-Parsons and 1.5 cm^{-1} for the Perkin-Elmer spectrophotometers, respectively.

ANALYSIS OF THE ABSORBANCE SPECTRA BY LORENTZ FUNCTIONS

The transmittance spectra of BSO, BGO, and BTO are shown in Fig. 1. The spectral range falls between 2000 and 1000 cm^{-1}, as all the samples show a strong absorption below 1000 cm^{-1}.

0740-3224/88/030714-07$02.00

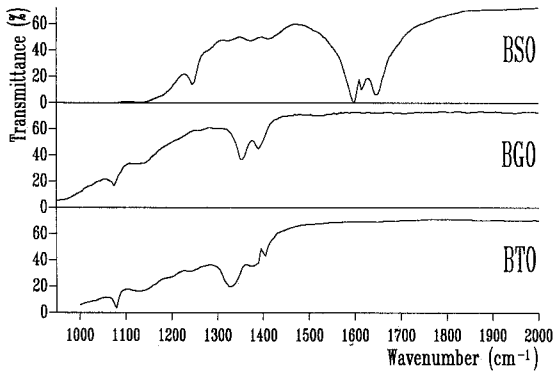

Fig. 1. Experimental transmittance spectra of BSO, BGO, and BTO single crystals.

To obtain accurate values for the band parameters—the position of the band maximum, the band half-width, and the band height—a multidimensional nonlinear regression was used, and a Lorentzian shape was assumed for each band. The procedure outlined by Horak and Vitek[9] has been adopted.

After converting transmittance values to absorbance values, the whole spectrum can be described by an mth-order-polynomial spectral background plus a superposition of a set of n Lorentz functions:

$$Y = \sum_{k=1}^{m+1} a_k \nu^{k-1} + \sum_{i=1}^{n} \frac{Y_{0,3i}}{[1 + b^2_{0,3i-2}(\nu - \nu_{0,3i-1})^2]}. \quad (1)$$

Each Lorentz function is characterized by three parameters: the band position ν_0 (cm^{-1}), the absorbance value at the band maximum Y_0, and the band half-width $\Delta\Gamma_0$; instead of $\Delta\Gamma_0$ we actually used the width parameter $b_0 = 2/\Delta\Gamma_0$ (cm).

In summary, the whole spectrum, which is made by a discrete set of points, (x_j, y_j) $j = \langle 1, N\rangle$, can be described as a function both of a $(1 + m + 3n)$-dimensional parameters vector $\mathbf{p}$ and of an N-dimensional vector $\mathbf{x}$ according to

$$Y = f(p_i, x_j) \qquad i = \langle 1, 1 + m + 3n\rangle; j = \langle 1, N\rangle. \quad (2)$$

Now it is necessary to find those components of the vector $\mathbf{p}$ that minimize the sum of the squared deviations. To increase the generalization, since the y_j values may be affected by errors expressed by their standard deviations, a multiplier weight diagonal matrix $\mathbf{W}$, whose terms are $w_{j,j} = 1/\sigma_j^2$, must be introduced. Hence the sum of the squared deviations takes the form

$$S = \sum_{j=1}^{N} w_{j,j} \left[y_j - \sum_{i=1}^{1+m+3n} f(p_i, x_j) \right]^2. \quad (3)$$

Among the available minimization methods, we have chosen the Newton–Raphson method, implemented by the Levenbergh damping method. To start the minimization process an initial estimate of all parameters must be given. If the set of the estimated parameters p_i^* is close to the correct solution, Eq. (2) can be expanded in a Taylor series as

$$Y = \left[f(\mathbf{p}, \mathbf{x}) + \sum_{i=1}^{1+m+3n} \frac{\partial f(\mathbf{p}, \mathbf{x})}{\partial p_i} (p_i - p_i^*) \right]_{\mathbf{p} = \mathbf{p}^*}; \quad (4)$$

hence

$$S = \mathbf{W}[Y^* - f(\mathbf{p}^*, \mathbf{x})] = \sum_{j=1}^{N} w_{j,j} + \left[\sum_{i=1}^{1+m+3n} \frac{\partial f(\mathbf{p}, \mathbf{x})}{\partial p_i} (p_i - p_i^*) \right]_{\mathbf{p} = \mathbf{p}^*}. \quad (5)$$

Moreover, the partial derivatives may be substituted by the Jacobian matrix $\mathbf{J}$,

$$\mathbf{W}[Y^* - f(\mathbf{p}^*, \mathbf{x})] = \mathbf{W}\mathbf{J}\Delta\mathbf{p}, \quad (6)$$

whose elements for the Lorentz bands are given by

$$J(\nu_0)_{j,3i-2} = \frac{2Y_{0i}b_{0i}^2(\nu_j - \nu_{0i})}{[1 + b_{0i}^2(\nu_j - \nu_{0i})^2]^2},$$

$$J(b_0)_{j,3i-1} = -\frac{2Y_{0i}b_{0i}(\nu_j - \nu_{0i})}{[1 + b_{0i}^2(\nu_j - \nu_{0i})^2]^2},$$

$$J(Y_0)_{j,3i} = \frac{1}{[1 + b_{0i}^2(\nu_j - \nu_{0i})^2]^2}, \quad (7a)$$

where $i = \langle 1, n\rangle$ and $j = \langle 1, N\rangle$, and those elements for the background are given by the polynomial derivatives

$$J(\nu_0)_{j,3n+k} = k a_{k+1} \nu^{k-1}, \quad (7b)$$

where $j = \langle 1, N\rangle$ and $k = \langle 1, m + 1\rangle$. This overdetermined system of N equations with $(1 + m + 3n) < N$ unknowns can be solved, after its conversion into a system of normal equations, by using the transposed Jacobian $\mathbf{J}^T$:

$$\mathbf{J}^T\mathbf{W}[Y^* - f(\mathbf{p}^*, \mathbf{x})] = \mathbf{J}^T\mathbf{W}\mathbf{J}\Delta\mathbf{p}, \quad (8)$$

that is,

$$\Delta\mathbf{p} = \frac{\mathbf{J}^T\mathbf{W}[Y^* - f(\mathbf{p}^*, \mathbf{x})]}{\mathbf{J}^T\mathbf{W}\mathbf{J}}. \quad (9)$$

The values obtained for $\Delta\mathbf{p}$ may be employed to calculate a new, better estimate of the parameter vector by

$$\Delta\mathbf{p}'^* = \mathbf{p} + \Delta\mathbf{p}. \quad (10)$$

When we start from Eq. (6), the calculation procedure must be repeated, and the iteration process continues until convergence between calculated and experimental Y values is reached. Sometimes the iteration process diverges because Eq. (1) is strongly nonlinear, and its approximation by a Taylor expansion, limited only to the first derivative term, is rough. To ensure convergence, it is necessary to introduce a damping factor h into the iteration process.

According to the Levenbergh method, the matrix $\mathbf{J}^T\mathbf{J}$ can be modified just by adding h to each diagonal term; the value for h must be chosen empirically. In such a way, the new matrix, $\mathbf{B} = \mathbf{J}^T\mathbf{J} + h\mathbf{U}$, where $\mathbf{U}$ is the unit matrix, will be generated. The damping-factor value changes automatically during computation, and the iteration procedure stops when one of the following events occurs:

(1) The preset value for the sum of the squared deviations is reached.

(2) The preset maximum number of iterations, typically 100, is reached.

(3) The convergence is not reached after a preset number of damping-factor modifications (typically 20).

As the regression program has sometimes shown a tendency to choose a linear background, we prefer to start the regression process with a best estimate of the background parameters. To do this, we selected a suitable set of background points at 100 cm^{-1} intervals, and then we applied a polynomial regression whose degree could be limited to 5–6. This procedure gives a first set of background parameters, which has been introduced in the file of the regression starting parameters.

Using the subroutines suggested by Horak and Vitek,[9] we have written a program in Fortran 77 for our HP 2000 Data System connected to a HP 7475A plotter. The program uses keyboard entries and works on data files stored on a hard disk.

BAND PARAMETERS DETERMINATION

The experimental and calculated absorbance spectra together with the background lines are shown in Figs. 2–4. For comparison, the single Lorentzian bands also are presented in the bottom of each figure. The absorbance values shown correspond to samples with thicknesses of 0.075 cm for BSO, 0.025 cm for BTO, and 0.020 cm for BGO.

In Table 1 the band parameters as given by each spectrum fitting with a set of Lorentz functions are reported. We have put those bands that seem to correspond on the same row.

As is usual for this kind of compound, the wave-number position for BSO bands is quite different from those of BGO and BTO samples. In fact, the band position decreases in the order BSO, BGO, BTO, according to the covalent radii increase of Si (0.117 nm), Ge (0.122 nm), and Ti (0.146 nm). The same increase may be found in the atomic distances in the crystals and is present also in the lattice constant values: 1.0104 nm for BSO, 1.0145 nm for BGO, and 1.0177 nm for BTO.[10] Nevertheless, for BGO and BTO samples the difference in the band position is not so evident as for BSO.

Because the Ge atom has larger size and atomic weight (72.59) than the Si atom (28.09), the BGO vibration frequencies must be lower than those of BSO. On the contrary, the Ti atom is larger than Ge, but its atomic weight (47.90) is lower than that of Ge. This relationship explains why, in certain spectral regions, the position of the BGO energy bands precedes that of the BTO energy bands, while in other regions the relative position is reversed.

In the analyzed spectral region the preeminent features are as follows. The BSO spectra show two intense bands at 1598 and 1649 cm^{-1}, with a relative amplitude of 1 to 0.355, plus a weak and narrow band at 1615 cm^{-1}. A similar band structure is evident in the BTO spectra, in which two intense peaks are located at 1330 and 1380 cm^{-1}, with a relative amplitude of 1 to 0.365, and a weak and narrow band is present at 1405 cm^{-1}. In the BGO spectra, only two bands are present at 1354 and 1392 cm^{-1}, with a relative amplitude of 1 to 0.615; other bands (numbers 1, 6, and 7 in Table 1) are extremely weak. These results are in partial agreement in wave number with the bands reported by Senulienė *et al.*[11] for BSO and BTO.

Another group of bands exists that seems to be interrelated, namely, the BSO bands at 1135 and 1179 cm^{-1}, the BGO bands at 1076 and 1143 cm^{-1}, together with the BTO bands at 1079 and 1140 cm^{-1}. Other bands (numbers 1, 6, 7, 11, and 12 in Table 1), which are probably due to overtones, are extremely weak.

For BSO, BGO, and BTO crystals, which belong to the space group T^3 (I23), it has been shown that there are 8 nondegenerate A modes, 8 doubly degenerate E modes, and 25 triply degenerate F modes.[12] All modes are Raman active, while only 24, belonging to the F symmetry, are infrared active.[13]

Wojdowski[13] has observed 23 F modes in BSO and 20 F modes in BGO at room temperature, and Zaretskii *et al.*[10]

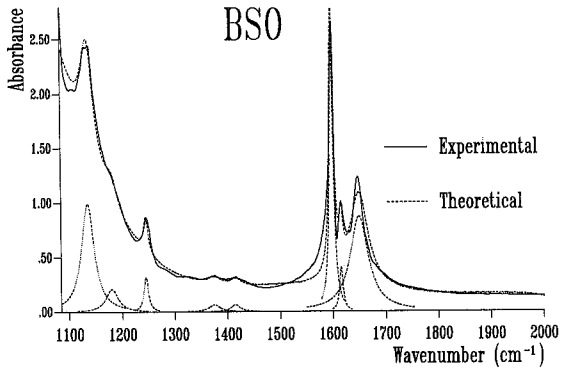

Fig. 2. Comparison of experimental and theoretical absorbance spectrum of BSO. The lowest curves represent the contribution of single Lorentzian functions.

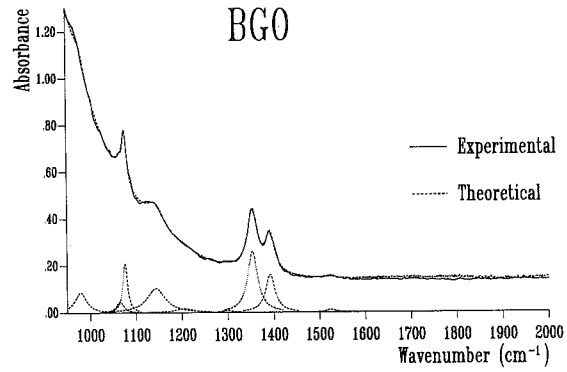

Fig. 3. Comparison of experimental and theoretical absorbance spectrum of BGO. The lowest curves represent the contribution of single Lorentzian functions.

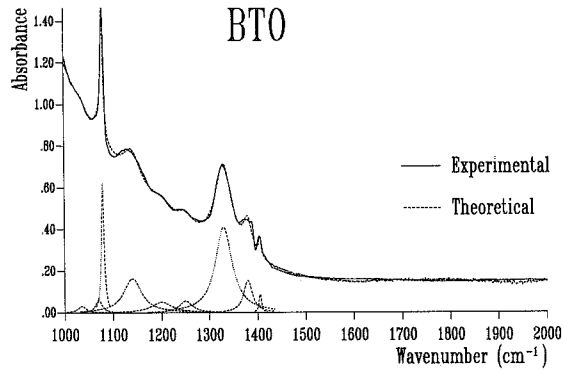

Fig. 4. Comparison of experimental and theoretical absorbance spectrum of BTO. The lowest curves represent the contribution of single Lorentzian functions.

Table 1. Values of Room-Temperature Band Parameters Given by the Lorentz Best Fit

BSO			BGO			BTO			
ν (cm^{-1})	Y_0	BW (cm^{-1})	ν (cm^{-1})	Y_0	BW (cm^{-1})	ν (cm^{-1})	Y_0	BW (cm^{-1})	Order Number
			1525	0.01	22				1
						1405	0.09	6	2
1650	0.87	42	1392	0.16	25	1380	0.15	22	3
1616	0.41	8							4
1598	2.45	9	1354	0.26	26	1330	0.41	43	5
1415	0.06	21	1300	0.01	25	1250	0.06	33	6
1375	0.06	24	1205	0.02	50	1200	0.05	51	7
1245	0.32	10	1143	0.10	48	1140	0.16	44	8
1180	0.21	28							9
1135	1.00	29	1076	0.21	12	1079	0.62	7	10
			1065	0.05	19	1070	0.06	16	11
			979	0.09	30	1035	0.03	20	12

have reported for BTO a Raman spectrum at 10 K without modes identification.

At present we have made no theoretical calculation of the vibrational frequencies to recognize the nature of the bands that we saw in the range 2000–1000 cm^{-1}. All these bands are probably due to overtones or combinations of the fundamental overtones. Indeed, a search made by Venugopalan and Ramdas[12] in BGO and BSO at 15 K revealed no Raman line between 850 and 3000 cm^{-1}. Nevertheless, there is little probability that some F modes, not previously reported, should be placed in this spectral region even if some modes could also be placed in the unexplored far-infrared region below 200 cm^{-1}.

ANALYSIS OF REFLECTANCE SPECTRA BY CLASSICAL OSCILLATORS

The experimental room-temperature reflectance spectra of BSO, BGO, and BTO are shown in Fig. 5. The BGO and BSO spectra are in particularly good agreement with the data reported previously by Wojdowski *et al.*,[14] at least in the range 800–500 cm^{-1}. In the region near 400 cm^{-1}, the data reliability is limited because the experimental system is close to its operative limits.

All spectra exhibit a number of reflection bands, which we assume to be due to the interaction of infrared radiation with the first-order electric dipole moment produced by the lattice modes at the center of the Brillouin zone. To test this hypothesis, we performed an analysis of the experimental data both in terms of the classical oscillator model and of the Kramers–Kronig relations. As pointed out by others,[15] both of these methods suffer from certain limitations.

The classic oscillator method may lead to ambiguities: in fact, in some cases different sets of oscillator parameters can satisfactorily fit the same spectrum.[16] Moreover, the fitting procedure may introduce spurious structures in the theoretical curve; these structures are not present in the experimental spectra.[15,17]

On the other hand, the Kramers–Kronig analysis requires that we know the reflection coefficient over the whole spectrum of frequencies. Because any measurement is limited to a finite frequency range, the reflection curves must be extrapolated on both sides of the experimental interval. Different extrapolation procedures may lead to widely different values of the optical constants, hence the choice of proper functions is crucial.

For the analysis based on the classical oscillator method, we have tried to apply to the reflectance spectra the same fitting procedure used for the absorbance curves. Because the reflection coefficient is a very complicated function of the basic oscillator parameters, our program often was unable to reach convergence. Therefore, we carried out our fitting procedure through the computer program MINUIT, a system for function minimization developed at CERN,[18] which consists of a set of routines performing minimization by different methods.

On the other hand, the limited number of parameters that the available release of MINUIT can handle did not allow us to process more than five bands, both in reflectance and in absorbance. Therefore, we could not use this program to fit our absorbance curves, because our curves exhibit a higher number of structures.

Among the MINUIT routines, the one based on the simplex-search method of Nelder and Mead[19] gave a very satisfactory fit for all three compounds. The results of this analysis are reported in Figs. 6–8, which show good agreement between theoretical and experimental data as well as the absence of any spurious structure in the calculated spectra. By running the program with different starting values and different step sizes of the parameters, we have also ascertained the uniqueness of the set of fitting parameters.

The experimental data have been fitted by the theoretical

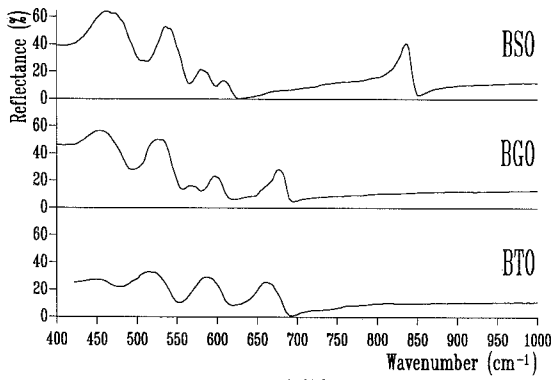

Fig. 5. Experimental reflectance spectra of BSO, BGO, and BTO single crystals.

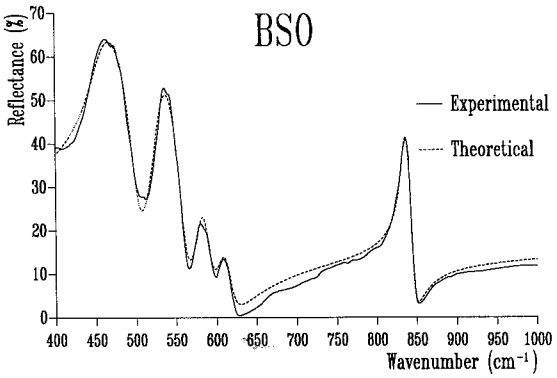

Fig. 6. Comparison of the experimental reflectance spectrum of BSO with the theoretical curve based on the classic oscillator model.

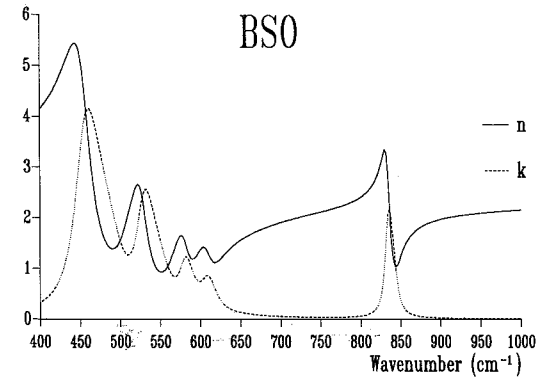

Fig. 9. Real (n) and imaginary (k) parts of the refractive index of BSO as given by the best-fit analysis of the reflectance spectrum.

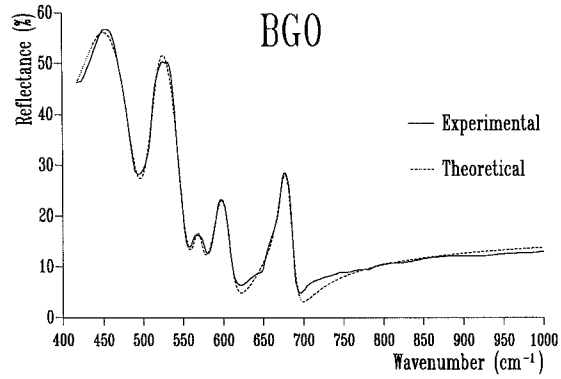

Fig. 7. Comparison of the experimental reflectance spectrum of BGO with the theoretical curve based on the classic oscillator model.

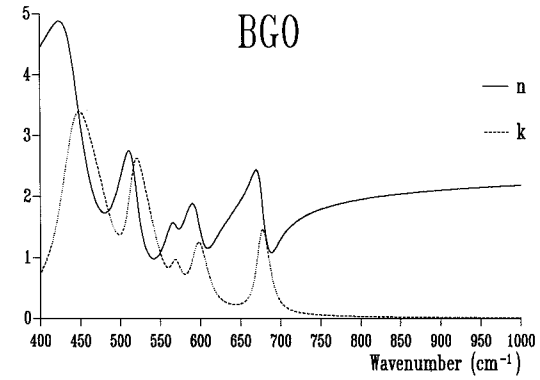

Fig. 10. Real (n) and imaginary (k) parts of the refractive index of BGO as given by the best-fit analysis of the reflectance spectrum.

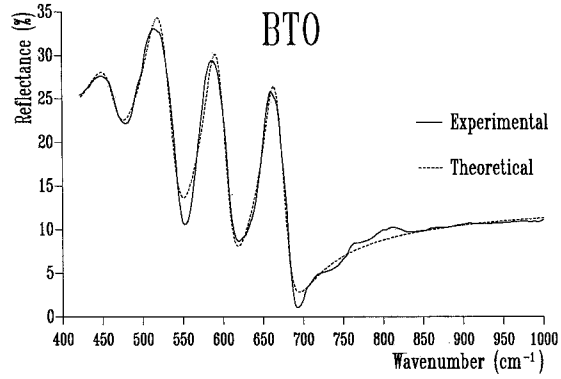

Fig. 8. Comparison of the experimental reflectance spectrum of BTO with the theoretical curve based on the classic oscillator model.

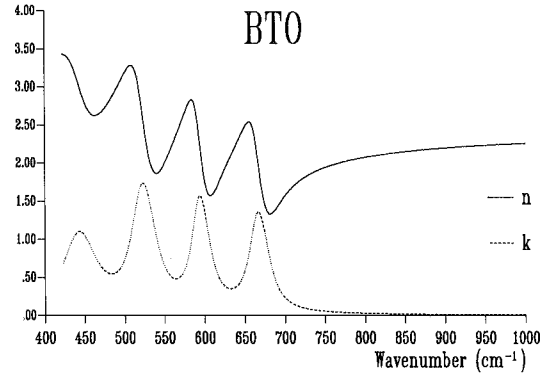

Fig. 11. Real (n) and imaginary (k) parts of the refractive index of BTO as given by the best-fit analysis of the reflectance spectrum.

Table 2. Values of Room-Temperature Classic Oscillator Parameters Given by the Best-Fit Procedure

BSO $n_0 = 2.307$			BGO $n_0 = 2.392$			BTO $n_0 = 2.150$		
ν (cm^{-1})	S	Γ (cm^{-1})	ν (cm^{-1})	S	Γ (cm^{-1})	ν (cm^{-1})	S	Γ (cm^{-1})
453	685.8	31	444	683.7	40	457	276.8	39
526	319.4	21	516	352.9	22	518	370.6	31
580	164.3	18	568	119.9	17	589	301.0	24
607	125.5	17	596	204.4	21	661	276.4	23
833	296.6	9	675	237.3	14			

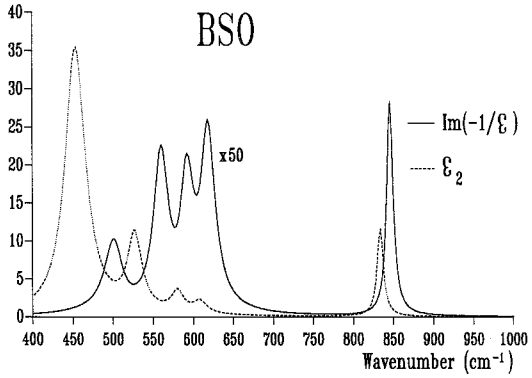

Fig. 12. Energy-loss function and imaginary part of the dielectric constant of BSO as given by the best-fit analysis of the reflectance spectrum.

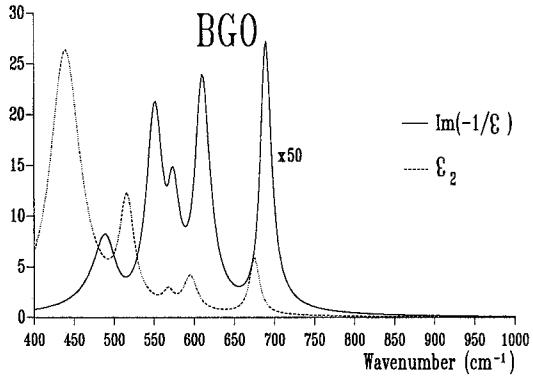

Fig. 13. Energy-loss function and imaginary part of the dielectric constant of BGO as given by the best-fit analysis of the reflectance spectrum.

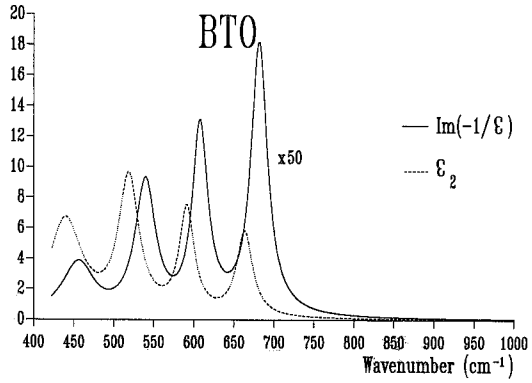

Fig. 14. Energy-loss function and imaginary part of the dielectric constant of BTO as given by the best-fit analysis and the reflectance spectrum.

expression of the reflectance as a function of the characteristic parameters of classical oscillators. We started with the well-known formula

$$R = \frac{1 + (\epsilon_1^2 + \epsilon_2^2)^{1/2} - 2^{1/2}[\epsilon_1 + (\epsilon_1^2 + \epsilon_2^2)^{1/2}]^{1/2}}{1 + (\epsilon_1^2 + \epsilon_2^2)^{1/2} + 2^{1/2}[\epsilon_1 + (\epsilon_1^2 + \epsilon_2^2)^{1/2}]^{1/2}}, \quad (11)$$

where the real and imaginary parts of the dielectric constant $\epsilon = \epsilon_1 + i\epsilon_2$ are related to the strength S_i, broadening Γ_i, and proper energy ν_i of the ith oscillator through the relations

$$\epsilon_1 = n_0^2 + \sum_i \frac{S_i^2(\nu^2 - \nu_i^2)}{(\nu^2 - \nu_i^2) + (\Gamma_i\nu_i)^2},$$

$$\epsilon_2 = \sum_i \frac{S_i^2\Gamma_i\nu_i}{(\nu^2 - \nu_i^2) + (\Gamma_i\nu_i)^2}. \quad (12)$$

S_i, Γ_i, and ν_i as well as the static refractive index n_0 were regarded as free parameters for the fitting procedure. The determination of these free parameters, which are listed in Table 2, allowed us to deduce theoretical values for all the optical constants of the crystal under study. In particular, the real **n** and imaginary **k** parts of the complex refractive index are shown in Figs. 9–11.

TO and LO modes are known to give rise to maxima in the functions ϵ_2 and $\mathrm{Im}(-1/\epsilon)$, respectively. Therefore, we focused our attention on these functions, which exhibit clearly defined structures, as shown in Figs. 12–14. In the absence of theoretical calculations of lattice modes, the existence of mode combinations cannot be excluded. In the frequency range of our experiment, five bands are observed for BSO and BGO, in agreement with the findings of other authors.[14] As shown in Table 3, the values of normal-mode energies are close to values obtained by Wojdowski *et al.*[14] when they applied Kramers–Kronig transformations to reflectance spectra. On the other hand, the spectra of BTO in the same frequency range show quite different features and, in particular, show the existence of only four bands.

As already mentioned, we also performed a Kramers–Kronig analysis of the reflectance curves, obtaining spectra of the optical constants ϵ_1 and ϵ_2, whose analytical expressions in terms of the basic oscillator parameters are quite simple. Such a procedure, however, gave unsatisfactory results because different extrapolation functions, mainly on the side of low energies, gave rise to very different values of the optical constants, and no valid criterion was found to establish which values were correct.

Discrepancies were found, mainly in the absolute values

Table 3. Normal-Mode Frequencies of BSO, BGO, and BTO, As Determined from the Reflectance Spectra at 300 K, Compared with Data from Wojdowski *et al.*[14]

	TO modes (cm^{-1})		LO modes (cm^{-1})	
Compound	Present Work	Ref. 14	Present Work	Ref. 14
BSO	453	458	501	506
	526	528	560	557
	579	576	592	591
	607	603	617	615
	833	822	846	838
BGO	444	455	488	493
	516	521	551	554
	568	572	574	578
	595	599	611	612
	675	680	689	690
BTO	457	–	467	–
	518	–	540	–
	589	–	608	–
	660	–	681	–

and overall line shapes of the dielectric constants, whereas the energy positions of the oscillators were much less sensitive to the choice of tail functions and were quite the same as those obtained by MINUIT. This observation explains the good agreement of the data shown in Table 3.

* Present address, Societá Italiana Sistemi Informativi Elettronici, via Isonzo 21/B, 00198 Rome, Italy.

REFERENCES

1. P. Vohl, P. Nisenson, and D. S. Oliver, "Real time incoherent to coherent optical converter," IEEE Trans. Electron Devices **ED-20,** 1032–1037 (1973).
2. J. O. White and A. Yariv, "Real time processing via four-wave mixing in a photorefractive medium," Appl. Phys. Lett. **37,** 5–7 (1980).
3. R. W. Whatmore, "New polar materials: their application to SAW and other devices," J. Cryst. Growth **48,** 530–547 (1980).
4. Sh. M. Efendiev, T. Z. Kulieva, V. A. Lomorov, M. I. Chigarov, M. Grandolfo, and P. Vecchia, "Crystal structure of bismuth titanium oxide $Bi_{12}TiO_{20}$," Phys. Status Solidi B **123,** k105–k108 (1984).
5. J. P. Huignard and J. P. Herriau, "Real-time coherent object edge reconstruction with $Bi_{12}SiO_{20}$ crystals," Appl. Opt. **17,** 2671–2672 (1978).
6. E. Burattini, G. Cappuccio, M. Grandolfo, P. Vecchia, and Sh. M. Efendiev, "Near infrared refractive index of bismuth germanium oxide ($Bi_{12}GeO_{20}$)," J. Opt. Soc. Am. **73,** 495–497 (1983).
7. G. Cappuccio, A. D'Amico, S. D'Angelo, and C. Ranghiasci, "Photometric linearity test for infrared spectrophotometers by means of a rotating sector disk attenuator," Appl. Opt. **21,** 3619–3622 (1982).
8. G. Cappuccio and S. D'Angelo, "Accessory for specular reflectance measurements with double-beam spectrophotometers," J. Phys. E **11,** 298–299 (1978).
9. M. Horak and A. Vitek, *Interpretation and Processing of Vibrational Spectra* (Wiley, New York, 1978).
10. Yu. G. Zaretskii, G. A. Kurbatov, V. V. Prokofev, Yu. I. Ukhanov, and Yu. V. Shmartsev, "Comparison of $Bi_{12}SiO_{20}$, $Bi_{12}GeO_{20}$, and $Bi_{12}TiO_{20}$ Raman spectra," Opt. Spectrosc. (USSR) **54,** 338–339 (1983) [Opt. Spektrosk. **54,** 569–571 (1983)].
11. D. Senulienė, G. Babonas, E. I. Leonov, I. Muminov, and V. M. Orlov, "Optical properties of $Bi_{12}Si_{1-x}Ti_xO_{20}$ single crystal," Phys. Status Solidi A **84,** 113–117 (1984).
12. S. Venugopalan and A. Ramdas, "Raman spectra of bismuth germanium oxide and bismuth silicon oxide," Phys. Rev. B **5,** 4065–4079 (1972).
13. W. Wojdowski, "Vibrational modes on $Bi_{12}GeO_{20}$ and $Bi_{12}SiO_{20}$ crystals" Phys. Status Solidi B **130,** 121–130 (1985).
14. W. Wojdowski, T. Lukasiewicz, W. Nazarewicz, and J. Zmija, "Infrared studies of lattice vibrations in $Bi_{12}GeO_{20}$ and $Bi_{12}SiO_{20}$ crystals," Phys. Status Solidi B **94,** 649–658 (1979).
15. V. K. Nagia, H. H. Soonpaa, and B. S. Rao, "Optical constants of bismuth tellurium sulfide," J. Opt. Soc. Am. **72,** 232–236 (1982).
16. H. W. Verleur, "Determination of optical constants from reflectance or transmittance measurements on bulk crystals or thin films," J. Opt. Soc. Am. **58,** 1356–1364 (1968).
17. B. W. Veal and A. P. Paulikas, "Optical properties of molybdenum. I. Experimental and Kramers–Kronig analysis," Phys. Rev. B **10,** 1280–1289 (1974).
18. F. James and M. Ross, "MINUIT—A system for function minimization and analysis of the parameter errors and correlations," Comput. Phys. Commun. **10,** 343–367 (1975).
19. J. A. Nelder and R. Mead, "A simplex method for function minimization," Comput. J. **7,** 308–313 (1965).